Journal of Rock Mechanics and Geotechnical Engineering 15 (2023) 1700–1712

Contents lists available at ScienceDirect

Journal of Rock Mechanics and Geotechnical Engineering

journal homepage: www.jrmge.cn

Full Length Article

A comparative study for determining rock joint normal stiffness with destructive uniaxial compression and nondestructive ultrasonic wave testing

Zhenghu Zhang [a,b], Jianbo Zhu [c,*], Jianhui Deng [d]

[a] School of Civil Engineering, Dalian University of Technology, Dalian, 116024, China
[b] Department of Civil and Environmental Engineering, The Hong Kong Polytechnic University, Hong Kong, China
[c] Guangdong Provincial Key Laboratory of Deep Earth Sciences and Geothermal Energy Exploitation and Utilization, College of Civil and Transportation Engineering, Shenzhen University, Shenzhen, 518060, China
[d] State Key Laboratory of Hydraulics and Mountain River Engineering, College of Water Resources and Hydropower, Sichuan University, Chengdu, 610065, China

ARTICLE INFO

Article history:
Received 19 June 2022
Received in revised form
21 August 2022
Accepted 16 October 2022
Available online 24 November 2022

Keywords:
Normal stiffness
Rock joint
Uniaxial compression
Ultrasonic wave

ABSTRACT

Rock joints are one of the vital discontinuities in a natural rock mass. How to accurately and conveniently determine joint normal stiffness is therefore significant in rock mechanics. Here, first, seven existing methods for determining joint normal stiffness were introduced and reviewed, among which Method I (the indirect measurement method), Method II (the direct determination method), Method III (the across-joint strain gauge measurement method) and Method IV (the deformation measuring ring method) are via destructive uniaxial compression testing, while Method V (the best fitting method), Method VI (the rapid evaluation method) and Method VII (the effective modulus method) are through wave propagation principles and nondestructive ultrasonic testing. Subsequently, laboratory tests of intact and jointed sandstone specimens were conducted following the testing requirements and procedures of those seven methods. A comparison among those methods was then performed. The results show that Method I, i.e. the benchmark method, is reliable and stable. Method II has a conceptual drawback, and its accuracy is acceptable at only very low stress levels. Relative errors in the results from Method III are very large. With Method IV, the testing results are sufficiently accurate despite the strict testing environment and complicated testing procedures. The results from Method V are greatly unstable and significantly dependent on the natural frequency of the transducers. The joint normal stiffness determined with Method VI is stable and accurate, although data processing is complex. Method VII could be adopted to determine the joint normal stiffness corresponding to the rock elastic deformation phase only. Consequently, it is suggested that Methods I, IV and VI should be adopted for the measurement of joint normal stiffness. The findings could be helpful in selecting an appropriate method to determine joint normal stiffness and, hence, to better solve discontinuous rock mass problems.

1. Introduction

Rock is a unique engineering material due to its inclusion of numerous discontinuities at various scales, among which the joint is the most important discontinuity type in many cases. Joints greatly affect the mechanical properties and engineering behaviors of a rock mass. For instance, the presence of joints could lower rock strength and stability of rock structures. Joint normal stiffness, which was first proposed by Goodman et al. (1968) to build a finite element model of a jointed rock block, is one of the key mechanical properties of a joint. Joint normal stiffness is usually an essential input parameter in rock mass problems, e.g. determining the deformation and stability of a rock mass or the seismic response of underground openings, in discrete element method-based modeling. As a result, it is very important to precisely obtain the joint normal stiffness in rock mechanics, engineering geology and applied geophysics.

* Corresponding author.
E-mail address: jianbo.zhu@szu.edu.cn (J. Zhu).
Peer review under responsibility of Institute of Rock and Soil Mechanics, Chinese Academy of Sciences.

https://doi.org/10.1016/j.jrmge.2022.10.010

Joint normal stiffness refers to the ratio of the axial applied stress to the corresponding axial displacement of the joint (Goodman et al., 1968). A typical axial stress–axial deformation curve of a rock joint is presented in Fig. 1. Since the normal deformation of the joint (u_n) presents a highly nonlinear increase with normal stress (σ_n), the definition of joint normal stiffness (k_n) should be expressed in differential form as

$$k_n = \frac{d\sigma_n}{du_n} \tag{1}$$

As shown in Fig. 1 and Eq. (1), joint normal stiffness is closely related to normal stress. Furthermore, joint normal stiffness is also susceptible to the geometry and mechanical properties of asperities of rough-walled joints, which can be characterized by joint roughness and contact area. Joint normal stiffness is empirically estimated according to established mathematical models using experimental data (Bandis et al., 1983; Goodman, 1989; Kulatilake et al., 2016). This paper focuses on the determination or measurement of joint normal stiffness and its influence factors.

It is usually a difficult job to precisely measure the joint normal stiffness of rock mass due to the three-dimensional (3D) attributes of joints and their complex surface topography (Bandis, 1980; Goodman, 1989; Zhu et al., 2018). Methods for measuring joint normal stiffness are divided into two types: destructive and nondestructive methods. Destructive methods are based on compression tests, while nondestructive methods are derived from wave propagation theory.

In destructive methods, joint normal stiffness is usually measured via a uniaxial compression test in laboratory or field (Goodman, 1974, 1976, 1989; Bandis et al., 1983; Raven and Gale, 1985; Jaeger et al., 2007; Nassir et al., 2010; Dang et al., 2017). Jointed rock specimens can be obtained by drilling a rock core perpendicular to the joint surface. Laboratory tests on the jointed rock specimens subjected to uniaxial compression are then carried out to acquire the joint normal stiffness. The axial displacement of the jointed rock is mainly attributed to the axial deformation of the joint, at least under low stress states. Consequently, joint normal stiffness is sometimes determined directly from the axial stress–displacement relationship of a jointed rock mass in engineering practice. However, the total axial deformation of jointed rock mass under uniaxial compression is constituted by the normal closure of the joint and the axial shortening of the two intact rock blocks (Goodman, 1976; Agharazi et al., 2012; Kulatilake et al., 2016), which means that the joint normal closure could be calculated by the total axial deformation minus the intact rock deformation. Hence, joint normal stiffness can be more accurately determined from the axial displacement–stress curves of joints. This is the most commonly used method (Bandis, 1980; Bandis et al., 1983; Barton et al., 1985; Cook, 1992; Malama and Kulatilake, 2003; Jaeger et al., 2007; Li et al., 2017). In addition, Daemen et al. (2004) proposed that joint normal stiffness could be measured from strain gauge measurement across the joint. In detail, the joint normal stiffness is acquired from the axial applied stress divided by the axial deformation corresponding to the strain gauge readings across the joint.

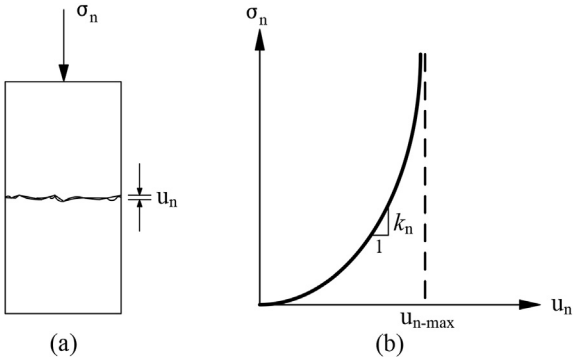

Fig. 1. Description of rock joint normal stiffness: (a) Sketch of normal loading on joint; and (b) A typical axial stress–deformation curve of a rock joint and the definition of normal stiffness.

Scholz and Hickman (1983) and Brown and Scholz (1986) used linear variable differential transducers (LVDTs) clamped to two frames, which were attached to a rock specimen, to measure the axial displacement of jointed rock between the frames, while that of intact rock with a length equal to the distance between the two frames was acquired from measurements of strain gauges glued to the specimen. The joint normal stiffness was determined as the ratio between the applied stress and the axial displacement of the joint, which is the difference between the axial displacement of the jointed rock between the frames and that of the intact rock with the identical length. Pyrak-Nolte (1988) measured joint displacement with one set of LVDTs spanning the fracture and another set of LVDTs spanning an equal length of intact rock. Cai (2001) applied steel rings mounted between two rectangular collars attached to rock specimens to measure joint normal stiffness. The similarity of these methods is that the joint normal stiffness is calculated by the across-joint deformation of a jointed rock minus the deformation of the intact rock with the same length.

Nondestructive methods to measure joint normal stiffness are via wave propagation theories, in particular, wave reflection and transmission at joints. Pyrak-Nolte et al. (1990) and Zhao et al. (2006) calculated joint normal stiffness with the best fitting results between theoretically estimated and experimentally measured amplitude spectra of transmitted waves through jointed rock in ultrasonic tests. Zhang et al. (2018) proposed a nondestructive approach to calculate the joint normal stiffness using the dominant frequency of transmitted waves. In addition, joint normal stiffness was solved by using an effective modulus model (Hart, 1993; Helm et al., 2013; Deng et al., 2015; Li et al., 2015). The dynamic elastic constants, namely, elastic modulus and Poisson's ratio, can be solved by compressional and shear wave velocities. Thus, it is reasonable to calculate joint normal stiffness using wave velocity.

There are a number of approaches for measuring joint normal stiffness. However, the advantages and disadvantages of these approaches are not yet well understood. Additionally, in practice, it is sometimes difficult to select an appropriate method to determine joint normal stiffness. Therefore, it is crucial to systematically review and compare different methods for the determination of joint normal stiffness and thereafter to make appropriate suggestions.

The objectives of this study are to review and compare seven methods for determining joint normal stiffness, in particular, to review and compare their applicability and accuracy to provide appropriate recommendations. First, seven existing methods to determine joint normal stiffness were summarized and classified, during which the procedures of different methods were formulated and standardized. Subsequently, destructive uniaxial compression and nondestructive ultrasonic tests were performed to determine joint normal stiffness with those seven methods. Finally, the joint normal stiffnesses determined with different methods were analyzed and compared. The merits and drawbacks of these existing approaches were also discussed. Suggestions for the utility of these methods were made thereafter. The findings could be beneficial to selecting an appropriate method to determine joint normal stiffness and hence to better solve problems related to rock masses.

2. Seven methods for determining joint normal stiffness

There are mainly seven approaches to measure joint normal stiffness. Methods I–IV are destructive and based on direct measurement of mechanical parameters from uniaxial compression tests, while Methods V–VII are based on nondestructive measurement of wave propagation using ultrasonic tests. Specifically, Methods V and VI are based on wave attenuation, while Method VII considers wave slowness.

2.1. Method I: Indirect measurement method

In Method I, the most common approach, joint normal stiffness is determined from the applied stress on the joint divided by the joint closure calculated by the axial deformation of the jointed rock mass minus that of an "identical" intact rock (Bandis, 1980; Bandis et al., 1983; Barton et al., 1985; Cook, 1992; Malama and Kulatilake, 2003; Jaeger et al., 2007). The axial deformations of intact and jointed rocks are determined by laboratory tests on intact and jointed rock specimens under uniaxial compression, respectively. The "identical" intact rock specimens are collected from the same rock core as the jointed rock specimens and have the same size as the jointed specimens. Method I is used as a benchmark to evaluate the other methods studied in this paper.

The axial deformation of jointed rock specimens is constituted by the axial deformations of joint and intact rock bearing a normal stress σ:

$$\mathrm{d}u_{\mathrm{eq}} = \mathrm{d}u_{\mathrm{ro}} + \mathrm{d}u_{\mathrm{n}} \tag{2}$$

$$\mathrm{d}u_{\mathrm{eq}} = \frac{\mathrm{d}\sigma}{k_{\mathrm{eq}}} \tag{3}$$

$$\mathrm{d}u_{\mathrm{ro}} = \frac{\mathrm{d}\sigma}{k_{\mathrm{ro}}} \tag{4}$$

$$\mathrm{d}u_{\mathrm{n}} = \frac{\mathrm{d}\sigma}{k_{\mathrm{n}}} \tag{5}$$

where u_{eq}, u_{ro} and u_{n} represent the axial deformations of jointed rock, intact rock and joint, respectively; and k_{eq}, k_{ro} and k_{n} symbolize the stiffnesses of jointed rock, intact rock and joint, respectively.

Thus, joint normal stiffness can be calculated as (Ingard and Kraushaar, 1960; Daemen et al., 2004):

$$k_{\mathrm{n1}} = \frac{k_{\mathrm{eq}}k_{\mathrm{ro}}}{k_{\mathrm{ro}} - k_{\mathrm{eq}}} \tag{6}$$

Note that the subscripts 1–7 denote the different methods studied in this paper.

Joint normal stiffness can be calculated by Eq. (6) or from the tangent of the axial stress–axial deformation curve of the joint.

In this paper, the axial deformation is measured by an LVDT with a measurement range of −2.5 mm to 2.5 mm. The testing procedures are as follows:

(1) Step 1: Laboratory tests of intact rock subjected to uniaxial compression to obtain the relationship between axial stress and axial deformation of intact rock; and
(2) Step 2: Laboratory tests of jointed rock subjected to uniaxial compression to acquire the relationship between axial stress and axial deformation of jointed rock.

Then, the axial stress-axial deformation curve and normal stiffness of the joint can be acquired.

2.2. Method II: Direct determination method

With Method II, joint normal stiffness is directly solved by the axial stress–displacement curve of the jointed rock mass. Joint normal stiffness at a specific stress is the tangent of the axial stress–displacement curve of the jointed specimen. The axial stress–deformation curve can be acquired from a laboratory test on a jointed rock specimen under uniaxial compression. The joint normal stiffness can be determined as follows:

$$k_{\mathrm{n2}} = \frac{\mathrm{d}\sigma}{\mathrm{d}u_{\mathrm{eq}}} \tag{7}$$

2.3. Method III: Across-joint strain gauge measurement method

In Method III, joint closure can be obtained by across-joint strain gauge measurement (Daemen et al., 2004). Specifically, joint displacement is the product of the axial strain across the joint (ε_{n}) and the length of the sensitive grid of the strain gauge (b):

$$\mathrm{d}u_n = b\mathrm{d}\varepsilon_{\mathrm{n}} \tag{8}$$

Then, the normal stiffness of the joint is calculated by

$$k_{\mathrm{n3}} = \frac{\mathrm{d}\sigma}{\mathrm{d}u_{\mathrm{n}}} = \frac{\mathrm{d}\sigma}{b\mathrm{d}\varepsilon_{\mathrm{n}}} \tag{9}$$

Fig. 2 shows the strain gauge layout pasted on the jointed rock specimen for Method III. Strain gauges 1–4 are used to measure axial deformation across the joint. Strain gauges 5 and 6 are utilized to obtain the axial deformation of the intact rock, while strain gauges 7 and 8 are utilized to obtain the lateral deformation. The length of the sensitive grid of each strain gauge is 5 mm.

2.4. Method IV: Deformation measuring ring method

With Method IV, joint closure is acquired from the axial deformation between the upper and lower walls of the joint minus that of the intact rock part with the identical length. Joint normal stiffness can then be determined by dividing the axial stress by joint closure (Goodman, 1976; Scholz and Hickman, 1983; Brown and Scholz,

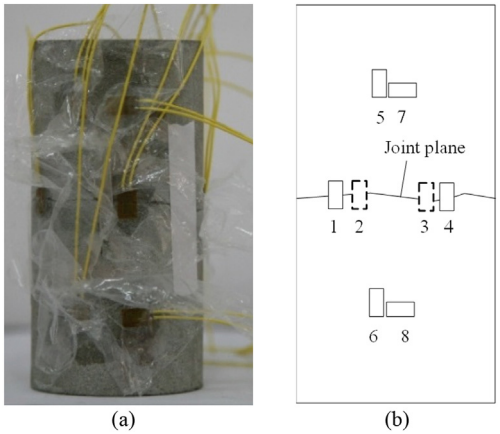

Fig. 2. Strain gauge installation for Method III: (a) Picture of strain gauge location; and (b) The strain gauge layout on the surface of the jointed rock specimen. Note that 1–4 are axial strain gauges across the joint; 5 and 6 are axial strain gauges on the intact rock; and 7 and 8 are lateral strain gauges on the intact rock blocks.

1986; Pyrak-Nolte, 1988; Cai, 2001). Although the testing and measurement methods used by different researchers slightly vary, they follow the same principle. Here, the method adopted by Cai (2001) is illustrated as an example. First, the accuracy ratio (α), the ratio between the readings of the strain gauge glued to the measuring rings and the diametrical displacement of the measuring rings, is acquired. Then, the relative axial displacement between the upper and lower walls of the joint (u_{eq4}) between the collars and the axial deformation of the joint can be solved:

$$du_{eq4} = d\varepsilon_{n4}/\alpha \tag{10}$$

$$du_{n4} = du_{eq4} - du_{ro4} = du_{eq4} - Dd\varepsilon_{ro4} \tag{11}$$

where ε_{n4} represents the strain of the measuring ring across the joint; u_{ro4} and ε_{ro4} refer to the displacement and strain of the intact rock component in an equal length of measuring ring, respectively; and D is the diameter of the measuring ring.

By solving Eqs. (10) and (11), the joint normal stiffness is determined by

$$k_{n4} = \frac{d\sigma_{eq}}{du_{n4}} = \frac{d\sigma}{d\varepsilon_{n4}/\alpha - Dd\varepsilon_{ro4}} \tag{12}$$

Two joint-deformation-measuring polyvinylchloride (PVC) rings, with diameters of 20 mm, were used to measure the axial deformation across the joint between two circular collars (Cai, 2001). Fig. 3 shows the working principle. Strain gauges are mounted to the PVC rings. The ratio of the reading of strain gauges to the radial displacement of the PVC rings is calibrated and obtained before testing. According to the calibration of the intact rock specimens, the PVC ring exhibits a sensitive and linear response to the joint deformation, and α is equal to 8.

2.5. Method V: Best fitting method

With Method V, joint normal stiffness can be calculated through obtaining the best fit between theoretical predictions and ultrasonic testing measurements of the amplitude spectra of transmitted waves across jointed rock mass (Pyrak-Nolte, 1988; Zhao et al., 2006; Zhu et al., 2011). First, transmitted waves across intact and jointed rocks are recorded in laboratory ultrasonic tests. To acquire amplitude spectra from the laboratory measurements, the fast Fourier transform (FFT) on the transmitted wave data is carried out. Then, the predicted amplitude spectra of the transmitted waves in jointed rock are derived via one-dimensional (1D) wave propagation theories and the transmission coefficient across a joint. The transmission coefficient (T) for vertically incident P-wave propagating through a single joint is expressed as (Schoenberg, 1980; Pyrak-Nolte et al., 1990):

$$T = \frac{2[k_n/(Z_p\omega)]}{-i + 2[k_n/(Z_p\omega)]} \tag{13}$$

where Z_p symbolizes the compressional wave impendence, i refers to the imaginary unit, and ω represents the angular frequency of the harmonic wave.

The joint normal stiffness can be acquired through the best fitting result between the theoretically predicted and laboratory measured spectra of jointed rock determined by trial and error.

2.6. Method VI: Rapid evaluation method

Zhang et al. (2018) proposed a rapid evaluation approach to calculate joint normal stiffness using the 1D plane wave theory, and this method is referred to as Method VI. By introducing a reasonable approximation to the wave equation solution, the joint normal stiffness is determined by (Zhang et al., 2018):

$$k_{n6} = \frac{Z_p\omega_t|T|}{2\sqrt{1-T^2}} \tag{14}$$

or

$$k_{n6} = \frac{Z_p\omega_t\sqrt{1-R^2}}{2|R|} \tag{15}$$

where ω_t represents the dominant frequency of the transmitted wave through the jointed rock, and R denotes the wave reflection coefficient.

Notably, Eq. (14) is derived from the transmission coefficient, while Eq. (15) is based on the reflected wave.

2.7. Method VII: Effective modulus method

Method VII is based on an effective modulus model and the relationship between the dynamic mechanical parameters and wave velocity. Joint normal stiffness can be acquired by the effective modulus model (Hart, 1993; Deng et al., 2015):

$$k_{n7} = \frac{E_{eq}E_{ro}}{(E_{ro} - E_{eq})H} \tag{16}$$

where E_{ro} represents the elastic modulus of intact rock, E_{eq} is the effective elastic modulus of jointed rock, and H symbolizes the height of intact or jointed rock.

The dynamic elastic constants, i.e. elastic modulus (E) and Poisson's ratio (μ), can be calculated by the compressional and shear wave velocities:

$$E = \rho V_p^2\frac{(1+\mu)(1-2\mu)}{1-\mu} \tag{17}$$

$$\mu = \frac{(V_p/V_s)^2/2 - 1}{(V_p/V_s)^2 - 1} \tag{18}$$

where V_p and V_s are the velocities of compressional and shear waves, respectively; and ρ is the density.

By solving Eqs. (16)–(18), the joint normal stiffness can be obtained.

3. Experimental setup

3.1. Specimen preparation

Because it is difficult to obtain several natural rock joints, whose planes are oriented perpendicular to the longitudinal axis of the cylindrical specimen and whose mechanical properties are similar, artificial rock joints produced by laboratory testing methods are used in this paper. There are several testing methods to fabricate artificial rock joint, e.g. sawing, hydraulic fracturing tests and point load tests. Compared to other methods, the point load test has the advantages of simple operation, high efficiency and low cost. When a joint surface is not normal to the specimen axes, the deformation of the joint includes normal and shear relative displacements. Since this study focuses on the joint normal stiffness, to guarantee that the joint deformation is in normal direction, the overall joint surface should be normal to the loading direction, namely, the specimen longitudinal axis. Two loading points are in the mid-plane of

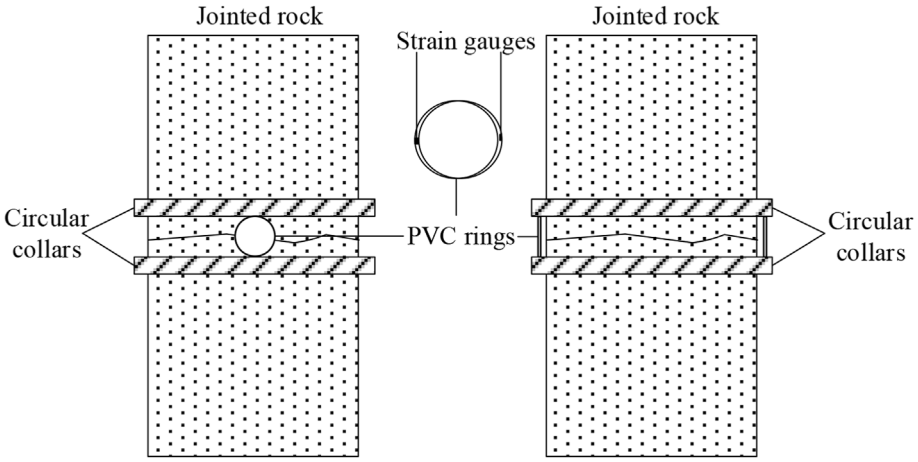

Fig. 3. Schematic of joint-deformation-measuring PVC rings.

specimens during point load tests, which can guarantee that ideal joints orthogonal to the longitudinal axis are prepared. As a result, point load tests are selected for producing artificial rock joint. In addition, overall flatness of joint surface after point load tests was tested. Specifically, four points equally distributed on the edge of each joint surface were selected. The distances between these points and their corresponding projection points on the end surface of specimens were measured. All distances must satisfy this condition that the range of distances is 50 mm ± 1 mm. Otherwise, the specimen will not be used for further laboratory tests.

Longchang sandstone is used in this study. Three groups of cylindrical jointed specimens were prepared, numbered S1-1 to S1-3, S2-1 to S2-3, and S1–S5, respectively, among which S1-1 to S1-3 are for Methods II and III, S2-1 to S2-3 are for Method IV, and S1–S5 are for Methods V–VII. Additionally, five intact rock specimens were fabricated from the identical rock core for use in the reference tests. There are no original natural cracks in the core. The mineral composition of sandstone specimens was tested by the charge coupled device (CCD) X-ray single crystal diffractometer (Model: Xcalibur E). The sandstone is constituted by several minerals, namely, quartz (37%), albite (51%), clinochlore (4%), phlogopite (7%) and calcite (1%). Fig. 4 illustrates intact and jointed specimens prepared from point load experiments and the typical surface morphology of a joint. The joint is located in the mid-plane of the specimens and oriented approximately perpendicular to the specimen longitudinal axis. The sizes of the cylindrical specimens are about 100 mm (height) × 50 mm (diameter). Both the two end surfaces of the rock specimens are smooth and flat. The density and uniaxial compressive strength (UCS) of the intact sandstone specimens are, on average, 2300 kg/m^3 and 56.28 MPa, respectively.

3.2. Experimental apparatus

A uniaxial compression machine and an ultrasonic testing system were used for this study. As shown in Fig. 5a, a rock mechanics testing machine (MTS815 Flex Test GT) is utilized to perform uniaxial compression tests. The loading rate is 10 kN/min. An OYO Sonic Viewer-SX was used to conduct ultrasonic testing and acquire transmitted pulses through intact and jointed rocks, as presented in Fig. 5b. The transmitter generates pulses with 500 V voltage and 6 μs ± 2 μs duration. Pulses in the frequency range of 10–1000 kHz can be well collected by the receiver. Three pairs of ultrasonic transducers, i.e. P 200 kHz, P 500 kHz and S 100 kHz, were used. Vaseline was utilized to guarantee a good connection between the specimens and ultrasonic transducers. The ultrasonic velocities of intact and jointed specimens were determined from the height of jointed specimen divided by the travel time in intact and jointed rock specimens. More details about this instrument can be found in the work of Zhang et al. (2018).

4. Results

4.1. Benchmark: Method I

The axial stress–deformation curves were acquired from uniaxial compression tests of intact and jointed specimens, respectively, from which the relationship between axial stress and axial deformation of the joint was derived by the total axial deformation of the jointed rock minus the intact rock shortening. Fig. 6 shows the typical relationship between axial stress and axial deformation of intact rock, jointed rock and joint. The joint normal stiffnesses are determined from the tangents of the axial stress–axial deformation curves of the joint at different axial stress levels, that is, the joint normal stiffnesses are ones at these particular stress levels. To eliminate the potential errors caused by fluctuations during force and displacement acquisition process, joint normal stiffness was calculated as the average value of 2 data before and after each of these particular stress levels. Fig. 7 illustrates the joint normal stiffnesses of specimens S1-1 to S1-3 and S2-1 to S2-3 under different axial stress levels obtained with the benchmark method (Method I). There are differences among joint normal stiffnesses of different specimens under same axial stress levels. For example, joint normal stiffnesses of specimens S1-1 to S1-3 under the axial stress of 1 MPa are 41.78 GPa/m, 31.74 GPa/m and 39.17 GPa/m, respectively. This is due to the discrepancy in joint surface morphology among different specimens. The joint normal stiffness grows with the applied stress level.

4.2. Methods II and III

In Method II, the joint normal stiffness was calculated directly from the axial stress and the corresponding deformation of the jointed rock specimen. Table 1 lists the joint normal stiffnesses determined with Method II of specimens S1-1 to S1-3 at different stress levels, and the relative errors between the results from Methods I and II are also included in Table 1. We found that the average relative errors between the joint normal stiffnesses determined with Methods I and II are 65.88%, 58.71% and 66.08% for specimens S1-1, S1-2 and S1-3, respectively, indicating an average

(a) (b)

Fig. 4. Sandstone specimens: (a) Specimens with numbers; and (b) The surface morphology of a joint.

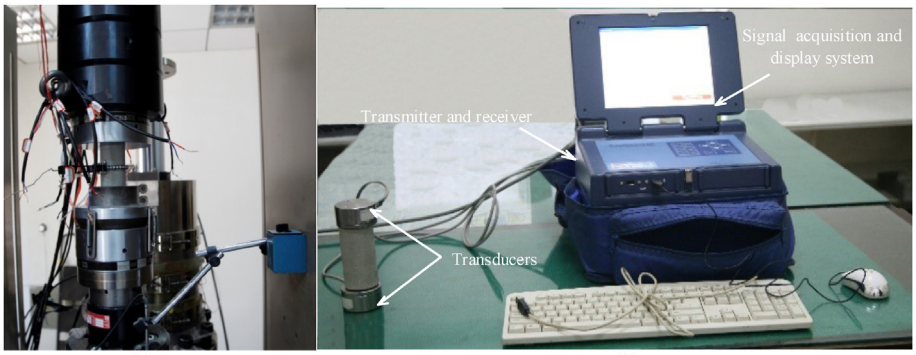

(a) (b)

Fig. 5. Test equipment: (a) MTS815 Flex Test GT rock mechanics testing system; and (b) The OYO Sonic Viewer-SX ultrasonic measuring system.

relative error of 63.56%. In addition, the relative error increases with increasing applied stress.

Fig. 8 illustrates the axial stress–deformation curves of the joints in specimens S1-1 to S1-3 acquired by Methods I and III. The axial displacements of joints measured with Method III are significantly less than those measured with Method I. Table 1 summarizes the joint normal stiffnesses derived by Methods I and III and their relative errors. The average relative errors between the joint normal stiffnesses acquired by Methods I and III for specimens S1-1, S1-2 and S1-3 are 2016.05%, 1919.75% and 2080.86%, respectively. The average relative error for all three specimens is 2005.56%.

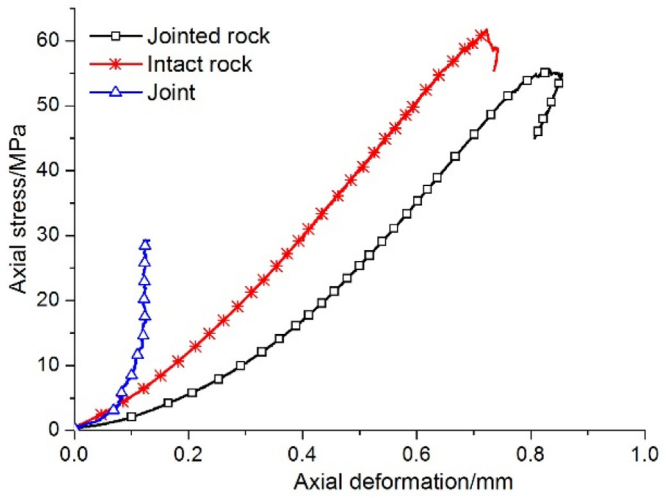

Fig. 6. Typical axial stress–deformation curves of intact rock, jointed rock and joint.

4.3. Method IV

Fig. 9 shows the axial stress–deformation curves of rock specimens S2-1, S2-2 and S2-3 obtained by Methods I and IV. The joint normal stiffness at different stress levels is listed in Table 2. The average relative errors between the joint normal stiffness of specimens S2-1, S2-2 and S2-3 acquired by Methods I and IV are 34.15%, 69.16% and 52.56%, respectively. The average relative error for all three specimens is 51.93%.

4.4. Methods V and VI

In Method V, tapering is needed to extract the initial transmitted pulse from the measured waveform. The selection and utilization of

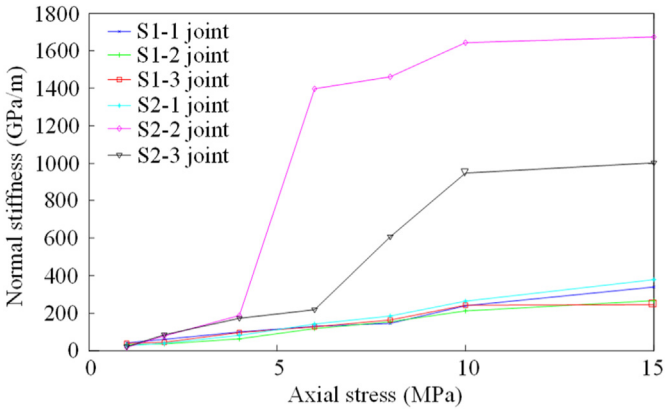

Fig. 7. Joint normal stiffness of specimens S1-1 to S1-3 and S2-1 to S2-3 under different axial stress levels with the benchmark method (Method I).

Table 1
Joint normal stiffness determined with Methods I–III.

Specimen	Axial stress (MPa)	Normal stiffness (GPa/m)			Relative error (%)	
		Method I	Method II	Method III	Method II	Method III
S1-1	1	41.78	16.34	1626.02	60.89	3791.62
	2	58.02	27.1	754.72	53.3	1200.81
	4	99.2	35.78	613.5	63.93	518.45
	6	127.91	42.81	963.86	66.53	653.52
	8	143.58	54.81	1503.76	61.83	947.33
	10	238.88	56.46	3738.32	76.36	1464.92
	15	337.98	73.37	19047.62	78.29	5535.72
	Average				65.88	2016.05
S1-2	1	31.74	18.51	358.42	41.69	1029.11
	2	34.08	19.17	408.16	43.75	1097.74
	4	63.37	36.56	1041.67	42.32	1543.68
	6	116.41	42.46	1581.03	63.53	1258.2
	8	153.07	46.35	2150.54	69.72	1304.96
	10	210.75	54.71	5333.33	74.04	2430.64
	15	264.74	63.67	12903.23	75.95	4773.92
	Average				58.71	1919.75
S1-3	1	39.17	20.73	1136.36	47.09	2800.8
	2	43.17	20.76	835.07	51.92	1834.31
	4	96.84	30.41	1473.3	68.6	1421.34
	6	126.81	42.26	2156.33	66.67	1600.45
	8	161.25	44.12	2657.81	72.64	1548.22
	10	241.82	47.14	5797.1	80.51	2297.24
	15	245.5	61.07	7766.99	75.12	3063.69
	Average				66.08	2080.86
All	Average				63.56	2005.56

tapering were presented in detail by the literature (Pyrak-Nolte et al., 1990; Zhao et al., 2006). Here, a half-sine taper with a window width and unitary amplitude is adopted by trial and error. Fig. 10 illustrates a typical original waveform, half-sine taper and tapered waveform. Fig. 11 shows the amplitude spectra of tapered transmitted waves from laboratory tests and those theoretically predicted by the best fit for specimens S1–S5, with P 200 kHz ultrasonic transducers. Similarly, Fig. 12 shows the amplitude spectra from the laboratory measurements and theoretical predictions with P 500 kHz ultrasonic transducers. The initial joint normal stiffness obtained from Method V is listed in Table 3. The average relative errors of the results from Method V measured by P-wave transducers with natural frequencies of 200 kHz and 500 kHz are 17.76% and 503.68%, respectively.

With Method VI, joint normal stiffness can be calculated by Eq. (14) or (15), which is dependent on three parameters, i.e., wave transmission or reflection coefficient, the P-wave impedance and dominant frequency of the transmitted wave across the joint. Table 4 shows the initial normal stiffness of the joint determined by Method VI. We found that the joint normal stiffnesses determined from Method VI via ultrasonic sensors with different natural frequencies are approximately identical, which indicates that the results from Method VI are stable regardless of the ultrasonic transducer frequencies. The average relative errors of the results from Methods I and VI determined by P 200 kHz and P 500 kHz sensors are 44.59% and 49.5%, respectively, as shown in Table 3.

4.5. Method VII

The dynamic elastic constants, including Poisson's ratio and elastic modulus, were respectively solved by Eqs. (17) and (18) using P- and S-wave velocities, which are summarized in Table 5. Here, P 500 kHz, P 200 kHz and S 100 kHz ultrasonic sensors were used. With the input parameters in Table 5 and Eq. (16), joint normal stiffness was determined and is presented in Table 6. Because the elastic modulus corresponds to the rock elastic deformation phase, the joint normal stiffness determined with Methods I and VII should be determined within this phase. Therefore, joint normal stiffness from Method I was determined under stresses ranging from 20% to 50% of the UCS. We found that the average relative errors between the joint normal stiffnesses determined with Methods I and VII measured by P-wave transducers with

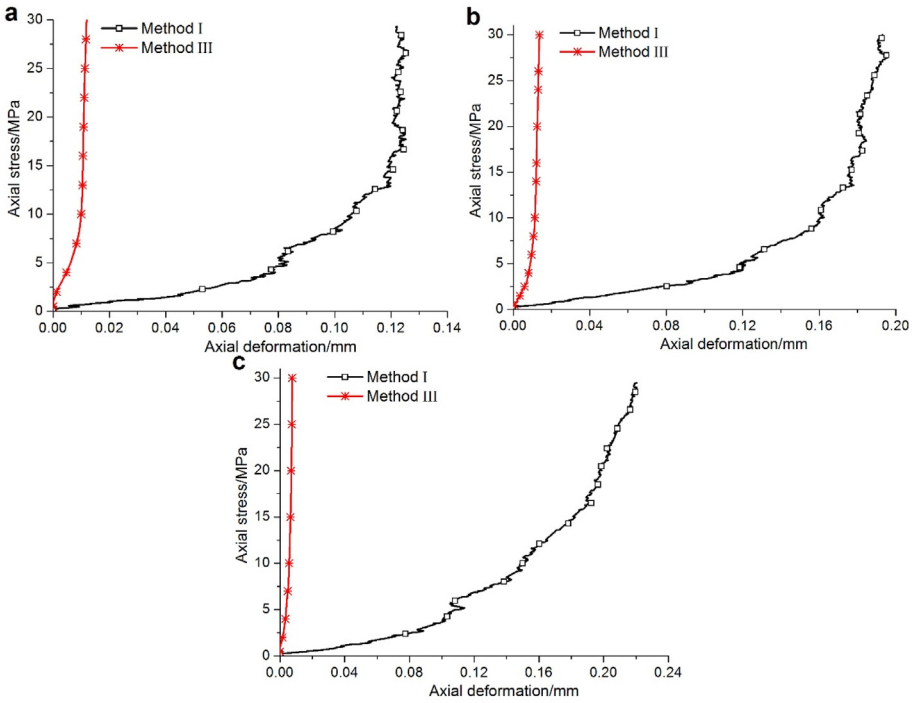

Fig. 8. Axial stress–deformation curves of joints acquired by Methods I and III: (a) specimen S1-1, (b) specimen S1-2, and (c) specimen S1-3.

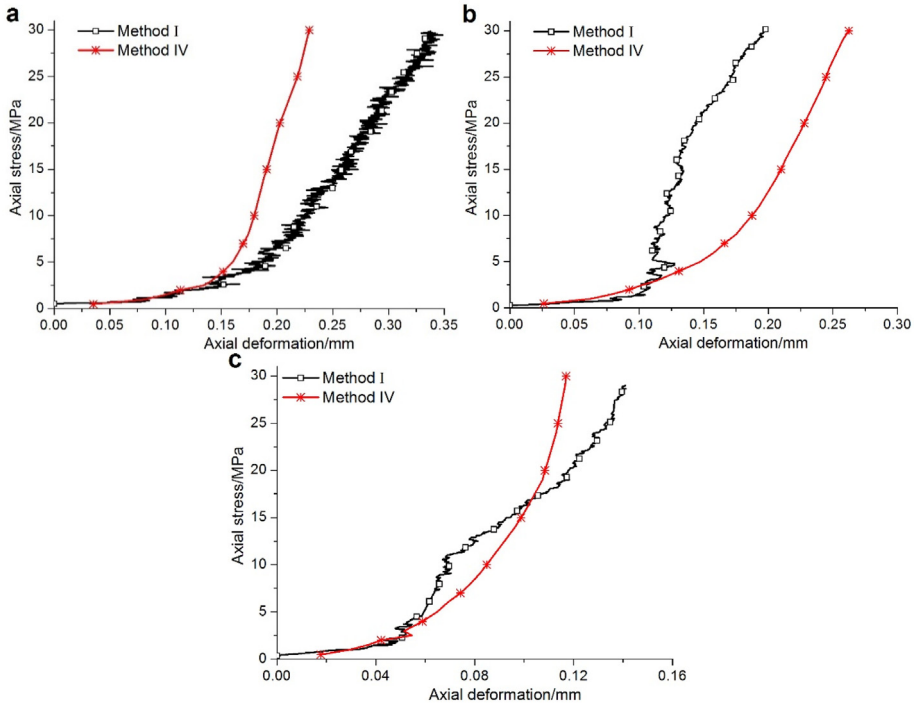

Fig. 9. Axial stress–deformation curves of joints obtained by Methods I and IV: (a) specimen S2-1, (b) specimen S2-2, and (c) specimen S2-3.

natural frequencies of 200 kHz and 500 kHz are 68.28% and 27.67%, respectively. As shown in Table 6, there are differences between the joint normal stiffnesses determined with Methods I and VII. The reason to cause the deviation from the two methods is that Method I is conducted from the uniaxial compressive test, while Method VII is from ultrasonic wave test. Furthermore, there are discrepancies between the joint normal stiffnesses of the same specimens via P-wave transducers with natural frequencies of 200 kHz and 500 kHz, which further indicates that the joint stiffness is frequency dependent.

Table 2
Joint normal stiffness determined with Methods I and IV.

Specimen	Axial stress (MPa)	Normal stiffness (GPa/m)		Relative error of Method IV (%)
		Method I	Method IV	
S2-1	1	25.07	15.46	38.34
	2	38.41	28.85	24.89
	4	79.72	103.76	30.15
	6	142.09	208.22	46.55
	8	183.36	281.76	53.67
	10	264.18	369.46	39.85
	15	379.24	400.53	5.61
	Average			34.15
S2-2	1	16.43	18.93	15.22
	2	77.13	41.99	45.56
	4	186.95	60.08	67.86
	6	1398.6	105.95	92.42
	8	1460.57	133.41	90.87
	10	1642.06	171.16	89.58
	15	1675.08	291.33	82.61
	Average			69.16
S2-3	1	21.03	52.06	147.57
	2	83.37	56.6	32.10
	4	173.3	149.93	13.49
	6	216.42	213.9	1.16
	8	606.5	260.3	57.08
	10	947.25	341.69	63.93
	Average			52.56
All	Average			51.93

5. Comparison and discussion

Methods I–IV determine joint normal stiffness via direct measurement of axial stress and deformation in destructive uniaxial compression tests. In essence, the main difference among these four methods is their accuracy in obtaining the normal closure of joints.

As a benchmark method in this paper, Method I is easy to apply in the laboratory or field, and the data processing is straightforward and convenient. In addition, the joint normal stiffness determined with Method I is stable.

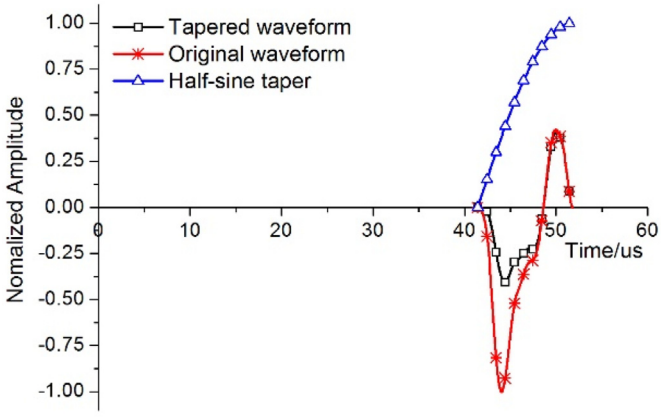

Fig. 10. Typical original waveform, half-sine taper and tapered waveform. Note that the pulse was normalized to peak amplitude prior to tapering.

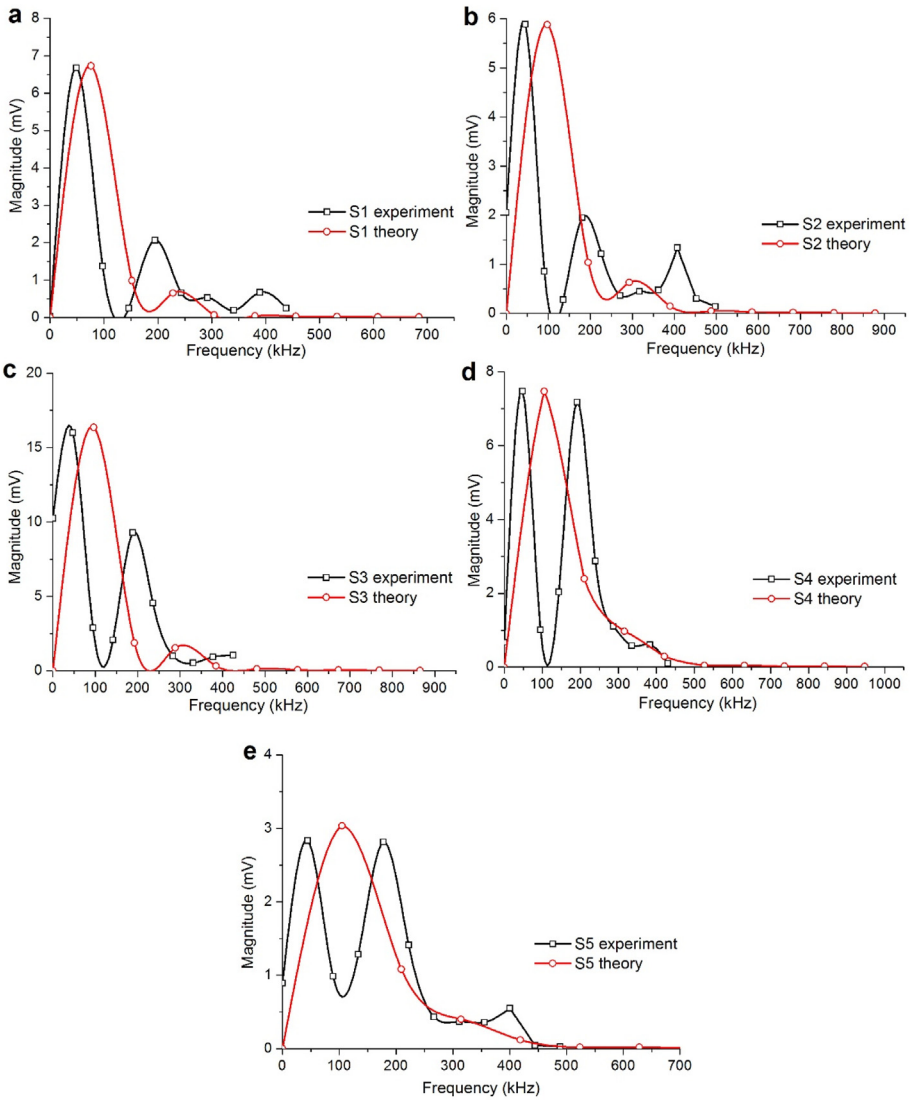

Fig. 11. Amplitude spectra obtained from laboratory measurements and theoretical predictions with P 200 kHz transducers: (a) specimen S1, (b) specimen S2, (c) specimen S3, (d) specimen S4, and (e) specimen S5.

Among the destructive Methods II–IV, the most accurate joint normal stiffness is measured with Method IV with an average error of 51.93% with respect to the results determined with the benchmark method, namely, Method I. Unlike Method I, in which axial deformation is measured by an LVDT, Method IV uses strain gauges to measure axial deformation. Compared with Method I, Method IV requires stricter testing conditions, such as a certain strain gauge direction, measuring ring and strain gauge connection and temperature, and has more complicated measuring processes, including the fabrication of the measuring rings and circular collars, the calibration of the measuring rings in intact rock, and the computation of the force and time conversion. In addition, the use of circular collars in Method IV could slightly affect the accuracy of the measured UCS and maximum displacement. The relative errors for Method IV probably result from the conversion between strain gauge readings and axial deformation. The axial displacement across the joint is indirectly measured by the readings of strain gauges glued to the measuring rings by Eqs. (10) and (11).

Although Method II does not subtract the axial displacement of the intact rock component from the total axial displacement of the jointed rock, its accuracy is acceptable, to some extent, with an average relative error of 63.56%. The accuracy of Method II in determining joint normal stiffness is acceptable at engineering scale when the stress level, e.g. in situ stress, is below 10% of the UCS or joint closure is less than half of the maximum closure. However, the relative error with respect to Method I increases significantly with increasing stress. The joint normal stiffness determined with Method II could be one order lower than that determined with Method I because the axial displacement of jointed rock mostly results from the axial deformation of the joint at lower stress levels, while the axial deformation of the intact rock plays a more important role with the increasing stress.

Relative errors of the joint normal stiffness determined with Method III are so high (2005.56% on average) that it is inapplicable to measure joint normal stiffness. This result may be because the strain gauge is not capable of measuring the deformation of the joint, which is much larger than the deformation of the material. The strain gauges usually work well in only the elastic deformation range. Therefore, even though the strain gauges provide accurate strains and deformations for relatively hard intact rock in the elastic deformation range, significant errors exist in measuring joint deformations that are highly nonlinear. Hence, the accuracy of the

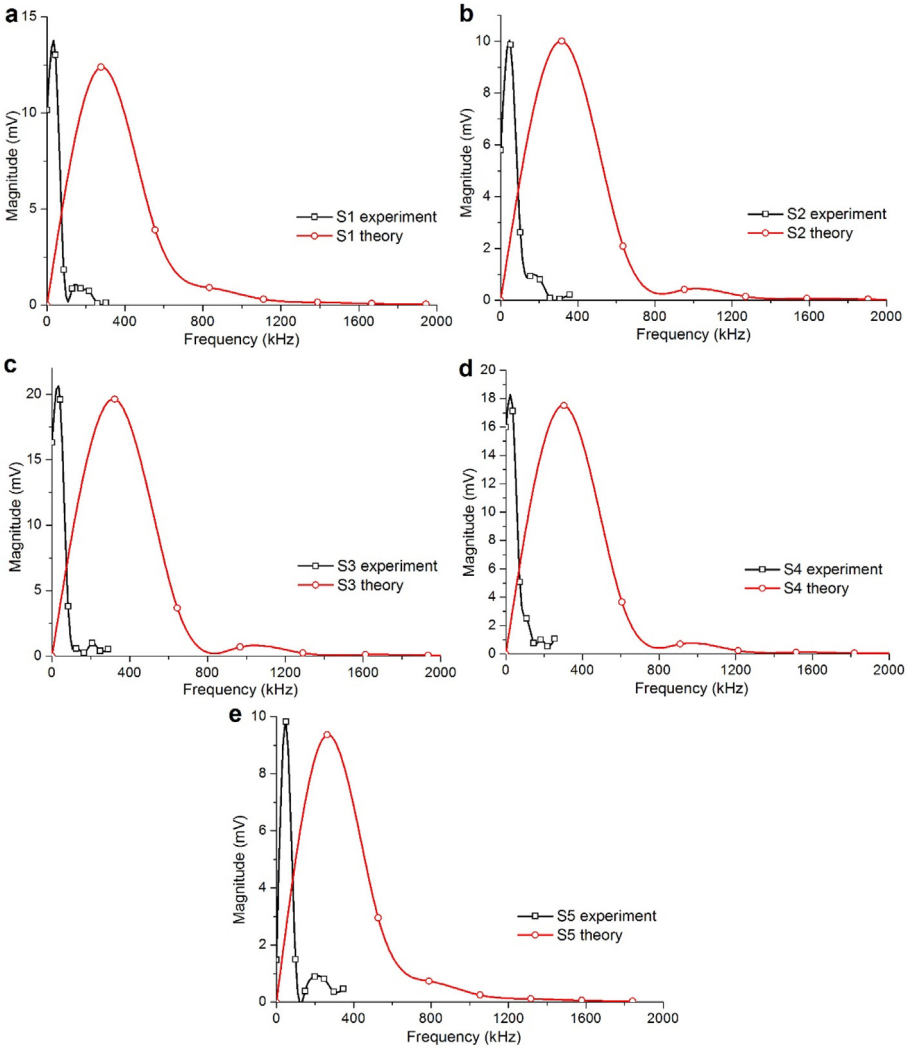

Fig. 12. Amplitude spectra obtained from laboratory measurements and theoretical predictions with P 500 kHz transducers: (a) specimen S1, (b) specimen S2, (c) specimen S3, (d) specimen S4, and (e) specimen S5.

estimated joint normal stiffness values based on Method III is highly questionable. Although strain gauge measurement was also used in Method IV, the stiffness acquired by Method IV has a high precision because the deformation measuring rings used in Method IV are always in the elastic deformation stage under normal loading. Hence, the strains measured by the strain gauges glued on the deformation measuring rings are accurate, which is an advantage of Method IV over Method III.

Table 3
Initial normal stiffness determined by Methods I, V and VI.

Transducer type	Specimen	Initial normal stiffness (GPa/m)			Relative error (%)	
		Method I	Method V	Method VI	Method V	Method VI
P 200 kHz	S1	5.22	3.88	2.58	25.7	50.62
	S2	5.87	5.13	2.28	12.63	61.1
	S3	8.16	10	4.05	22.5	50.42
	S4	5.9	7.45	4.01	26.3	31.94
	S5	5.52	5.61	3.93	1.66	28.86
	Average	6.13	6.41	3.37	17.76	44.59
P 500 kHz	S1	5.22	16.09	1.7	208.1	67.36
	S2	5.87	36.69	3.01	524.85	48.68
	S3	8.16	56.11	3.71	587.36	54.54
	S4	5.9	42.03	3.23	612.54	45.26
	S5	5.52	37.83	3.77	585.54	31.65
	Average	6.13	37.75	3.09	503.68	49.5
All	Average				260.72	47.05

Table 4
Initial normal stiffness of joints determined with Method VI (Zhang et al., 2018).

Transducer type	Specimen	Wave impedance (10^6kg/(m^2 s))	Transmitted dominant frequency (kHz)	Transmission coefficient	Initial normal stiffness (GPa/m)
P 200 kHz	S1	5.57	48.66	0.02	2.58
	S2	5.45	45.25	0.02	2.28
	S3	5.55	47.17	0.03	4.05
	S4	5.5	47.85	0.03	4.01
	S5	5.43	44.44	0.03	3.93
	Average	5.5	46.67	0.03	3.37
P 500 kHz	S1	6.03	43.1	0.01	1.7
	S2	5.83	51.02	0.02	3.01
	S3	5.9	41.32	0.03	3.71
	S4	5.89	36.36	0.03	3.23
	S5	5.88	49.5	0.03	3.77
	Average	5.91	44.26	0.02	3.09

Table 5
Dynamic Poisson's ratio and elastic modulus calculated by P- and S-wave velocities.

Transducer type	Rock type	Specimen	V_p (m/s)	V_s (m/s)	ρ (g/cm^3)	μ	E (GPa)
P 200 kHz and S 100 kHz	Intact rock	S1	2418.38	1670.84	2.3	0.04	13.43
		S2	2385.17	1679.87	2.29	0.01	13
		S3	2414.96	1672.51	2.3	0.04	13.35
		S4	2390.42	1646.86	2.3	0.05	13.09
		S5	2364.93	1663.33	2.3	0.01	12.84
		Average	2394.77	1666.68	2.3	0.03	13.14
	Jointed rock	S1	2352.94	1562.5	2.3	0.11	12.44
		S2	2348.65	1582.54	2.29	0.08	12.41
		S3	2358.07	1640.98	2.3	0.03	12.75
		S4	2359.34	1535.38	2.3	0.13	12.29
		S5	2310.19	1584.13	2.3	0.06	12.17
		Average	2345.84	1581.11	2.3	0.08	12.41
P 500 kHz and S 100 kHz	Intact rock	S1	2617.8	1670.84	2.3	0.16	14.88
		S2	2549.87	1679.87	2.29	0.12	14.4
		S3	2569.96	1672.51	2.3	0.13	14.55
		S4	2558.97	1646.86	2.3	0.15	14.32
		S5	2562.26	1663.33	2.3	0.14	14.43
		Average	2571.77	1666.68	2.3	0.14	14.52
	Jointed rock	S1	2436.05	1562.5	2.3	0.15	12.95
		S2	2408.21	1582.54	2.29	0.12	12.82
		S3	2432.56	1640.98	2.3	0.08	13.39
		S4	2467.24	1535.38	2.3	0.18	12.85
		S5	2449.08	1584.13	2.3	0.14	13.14
		Average	2438.63	1581.11	2.3	0.14	13.03

Therefore, in addition to Method I, which is reliable in measuring joint normal stiffness, among destructive Methods II–IV, Method IV is the most accurate but has higher requirements for the testing conditions during the measuring process, Method II is an acceptable method at relatively low stress levels, and Method III is not suitable for determining joint normal stiffness because of its significant inaccuracy.

Nondestructive Methods V–VII are based on wave theories and ultrasonic tests. Methods V and VI are based on wave propagation, while wave slowness is taken into account in Method VII. The nondestructive methods have advantages over Methods I–IV by virtue of their nondestructive nature. However, the data processing for Methods V–VII is more complicated than that for Methods I–IV.

The relative errors of the initial normal stiffness with Method V measured by P-wave ultrasonic sensors with natural frequencies of 200 kHz and 500 kHz are 17.76% and 503.68%, respectively, indicating that the results from Method V are greatly unstable and dependent on the natural frequency of the transducers.

Unlike Method V, Method VI uses dominant frequencies of the transmitted wave across jointed rock mass to determine the joint normal stiffness. The dominant frequencies of a longitudinal wave (P-wave) transmitting across the jointed rock obtained by P 200 kHz and P 500 kHz ultrasonic sensors are on average 46.67 kHz and 44.26 kHz, indicating that the dominant frequencies of transmitted waves through a jointed rock specimen are approximately the same regardless of the natural frequency of the transducer or the incident wave. Therefore, the joint normal stiffness determined with Method VI is stable. In addition, the joint normal stiffness measured with Method VI is accurate and has an average error of 47.05% with respect to the benchmark method. The relative errors for Method VI may be attributed to the differences of loading rate (or frequency) and degree of joint deformation. The uniaxial compression tests for Method I are static or quasi-static, while ultrasonic wave tests used in Method VI are high-frequency seismic. Furthermore, the deformation of a joint under the uniaxial compressive loading is large compared to ultrasonic wave tests because the energy of the ultrasound is so low and therefore does not cause obvious joint deformation.

Based on wave slowness, Method VII determines joint normal stiffness from the dynamic elastic modulus in the elastic deformation phase of the rock specimens. The relative errors, i.e. 68.28% for a P 200 kHz transducer and 27.67% for a P 500 kHz transducer, are small. Therefore, its accuracy and reliability in determining joint normal stiffness are confirmed. However, shear ultrasonic transducers are needed in addition to compressional transducers. In addition, the derived results from Method VII are sensitive to the ultrasonic transducer frequency.

Among all seven methods, it is suggested that Method I (the indirect measurement method), Method IV (the deformation measuring ring method), and Method VI (the rapid evaluation method) should be used for measurement of joint normal stiffness, although the testing requirements in Method IV are strict, and the data processing in Method VI is complicated. The accuracy of Method II is acceptable at only low stress levels. Method VII (the effective modulus method) could be adopted to determine the joint normal stiffness corresponding to the rock elastic deformation phase only. Methods III and V, however, are not recommended because of their higher relative errors, unstable measurements or complicated solving processes, as listed in Table 7.

Priority is given to Method I for determining joint normal stiffness because of its explicit physical meaning and simple experimental operation. When rock masses are clearly heterogeneous and there are numerous preexisting microdefects in the rock specimens, Method IV is recommended to obtain the joint normal stiffness because all the deformations and stresses are measured in

Table 6
Joint normal stiffness determined with Methods I and VII.

Specimen	Normal stiffness (GPa/m)			Relative error (%)	
	Method VII		Method I		
	P 200 kHz	P 500 kHz		P 200 kHz	P 500 kHz
S1	1696.66	997.24	845.18	100.74	17.99
S2	2748.43	1170.87	1360.12	102.07	13.91
S3	2808.27	1671.76	2207.4	27.22	24.27
S4	2026.46	1257.73	1347.56	50.38	6.67
S5	2347.65	1473.14	6020	61	75.53
Average	2325.5	1314.15	2356.05	68.28	27.67

Table 7
Pro and con of seven existing methods for determining rock joint normal stiffness.

Method	Advantage	Disadvantage
I	Reliable, explicit physical meaning, and simple experimental operation	Destructive, and time-consuming
II	Rapid, and convenient	Destructive, conceptual drawback, and acceptable at only low stress levels
III	Convenient	Destructive, high relative errors, and unstable measurements
IV	Reliable, and explicit physical meaning	Destructive, high testing requirement, an dcomplicated solving processes
V	Nondestructive	Unstable, frequency dependent, and complicated solving processes
VI	Nondestructive, rapid, and reliable	Theoretical approximation
VII	Nondestructive, and reliable	Frequency dependent, and S-wave transducers needed

the same rock specimen. If the rock specimens must remain undamaged, Method VI is recommended for determining joint normal stiffness because it is a nondestructive and reliable testing method.

Joint normal stiffness is an important parameter for many jointed rock masses. For example, in discrete element models of a rock mass, joint normal stiffness is usually an input parameter (Fan et al., 2015; Jiang et al., 2015). In blasting or earthquake engineering, wave attenuation in a jointed rock mass mostly results from wave reflection at joints within the rock material, and the wave reflection at joints is dependent on the joint normal stiffness (Pyrak-Nolte, 1988; Cai, 2001; Zhao et al., 2012; Li, 2013; Zhu and Zhao, 2013; Li et al., 2014). Therefore, an appropriate method that could accurately and conveniently determine joint normal stiffness is essential.

In this paper, destructive uniaxial compression and nondestructive ultrasonic tests were conducted for a single rock type, i.e. sandstone, in which artificial joints were fabricated by splitting cylindrical specimens in point load tests. Additional studies with other rock types and natural rock joints could supplement our findings and further consolidate our conclusions. In our paper, a half-cycle sine wave is adopted as the taper for Method V. It is possible that the joint normal stiffness determined using other tapers could be more accurate. In addition, only joint normal stiffness is investigated in our research, and further study on joint shear stiffness is needed in the future.

6. Conclusions

In this study, different methods to determine joint normal stiffness were introduced and compared. The main conclusions drawn from the present investigation are as follows:

(1) Among the four destructive methods, Method I, namely, the indirect measurement method, determines the joint normal stiffness by dividing the stress by the joint closure and is adopted as the benchmark method. The accuracy of Method II, namely, the direct determination method, is acceptable at only low stress levels. The relative errors of the joint normal stiffness determined by Method III, i.e. the across-joint strain gauge measurement method, are so high that this method is inappropriate for measuring joint normal stiffness. The stiffness values determined by Method IV, namely, the deformation measuring ring method, are sufficiently accurate despite having strict testing requirements.

(2) Among the three nondestructive methods, the results from Method V, namely, the best fitting method, are greatly unstable and significantly dependent on the natural frequency of the transducer. With Method VI, namely, the rapid evaluation method, the determined joint normal stiffness is stable and relatively accurate, with an average error of 47.05%. The joint normal stiffness corresponding to the rock elastic deformation phase is measured with Method VII, namely, the effective modulus method, which is accurate and has an average relative error of 47.98%.

(3) According to their calculation precision and stability, among all seven methods, it is recommended that Methods I, IV and VI should be adopted for measurement of joint normal stiffness, although the requirements for the testing conditions of Method IV are strict, and the data processing in Method VI is complex. Methods II, III, V and VII, however, are not recommended because they involve higher relative errors, unstable measurements or complicated solving processes.

(4) In general, Method I is preferred for measuring joint normal stiffness. When rock masses are clearly heterogeneous and there are a great number of preexisting microdefects in the rock specimens, Method IV is recommended to acquire joint normal stiffness. If the rock specimens must remain undamaged, Method VI is suggested.

Declaration of competing interest

The authors declare that they have no known competing financial interests or personal relationships that could have appeared to influence the work reported in this paper.

Acknowledgements

This study is financially supported by the Shenzhen Fundamental Research Program (Grant No. JCYJ20220818095605012), the National Natural Science Foundation of China (Grant No. 51909026), and the Fund of Guangdong Provincial Key Laboratory of Deep Earth Sciences and Geothermal Energy Exploitation and Utilization (Grant No. 2020-08).

Abbreviations

k_n	Joint normal stiffness
σ	Axial stress
u_{ro}	Axial displacement of intact rock
u_{eq}	Axial displacement of jointed rock
u_n	Joint closure
k_{ro}	Axial stiffness of intact rock
k_{eq}	Axial stiffness of jointed rock
b	Length of sensitive grid of strain gauge
ε_n	Axial strain across the joint
α	Ratio between the reading of strain gauges and the radial deformation of measuring rings
D	Diameter of measuring ring
ε_{ro}	Axial strain of intact rock component
ω	Angular frequency
Z_p	P-wave impedance
R	Wave reflection coefficient
T	Wave transmission coefficient
ω_t	Dominant frequency of transmitted wave
ρ	Rock density
V_p	Phase velocity of compressional wave (P-wave)
V_s	Phase velocity of shear wave (S-wave)
H	Height of intact or jointed rock
E_{ro}	Elastic modulus of intact rock
E_{eq}	Effective elastic modulus of jointed rock
μ	Poisson's ratio

References

Agharazi, A., Martin, C.D., Tannant, D.D., 2012. A three-dimensional equivalent continuum constitutive model for jointed rock masses containing up to three random joint sets. Geomechanics Geoengin. 7 (4), 227–238.

Bandis, S., 1980. Experimental Studies of Scale Effects on Shear Strength, and Deformation of Rock Joints. PhD Thesis. University of Leeds, Leeds, UK.

Bandis, S.C., Lumsden, A.C., Barton, N.R., 1983. Fundamentals of rock joint deformation. Int. J. Rock Mech. Min. Sci. Geomech. Abstr. 20 (6), 249–268.

Barton, N., Bandis, S., Bakhtar, K., 1985. Strength, deformation and conductivity coupling of rock joints. Int. J. Rock Mech. Min. Sci. Geomech. Abstr. 22 (3), 121–140.

Brown, S.R., Scholz, C.H., 1986. Closure of rock joints. J. Geophys. Res. Solid Earth 91 (B5), 4939–4948.

Cai, J.G., 2001. Effects of Parallel Fractures on Wave Attenuation in Rock. PhD Thesis. Nanyang Technological University, Singapore.

Cook, N.G.W., 1992. Natural joints in rock: mechanical, hydraulic and seismic behaviour and properties under normal stress. Int. J. Rock Mech. Min. Sci. Geomech. Abstr. 29 (3), 198–223.

Daemen, J.J., Danko, G., Smiecinski, A.J., 2004. Experimental Determination of Stiffness of Joints in Welded Tuff. Technical Report. University of Nevada, Reno, USA.
Dang, W., Konietzky, H., Frühwirt, T., 2017. Direct shear behavior of planar joints under cyclic normal load conditions: effect of different cyclic normal force amplitudes. Rock Mech. Rock Eng. 50 (11), 3101–3107.
Deng, X.F., Chen, S.G., Zhu, J.B., Zhou, Y.X., Zhao, Z.Y., Zhao, J., 2015. UDEC–AUTODYN hybrid modeling of a large-scale underground explosion test. Rock Mech. Rock Eng. 48 (2), 737–747.
Fan, X., Kulatilake, P.H.S.W., Chen, X., 2015. Mechanical behavior of rock-like jointed blocks with multi-non-persistent joints under uniaxial loading: a particle mechanics approach. Eng. Geol. 190, 17–32.
Goodman, R.E., Taylor, R.S.L., Brekke, T.L., 1968. A model for the mechanics of jointed rock. J. Soil Mech. Found Div. 94 (3), 637–659.
Goodman, R.E., 1974. The mechanical properties of joints. In: Advances in Rock Mechanics: Proceedings of the 3rd Congress of the International Society for Rock Mechanics, vol. 1. National Academy of Sciences, Washington, D.C., USA, pp. 127–140.
Goodman, R.E., 1976. Methods of Geological Engineering in Discontinuous Rocks. West Publishing, Saint Paul, USA.
Goodman, R.E., 1989. Introduction to Rock Engineering, second ed. Wiley, New York, USA.
Hart, R.D., 1993. An introduction to distinct element modeling for rock engineering. In: Hudson, J.A. (Ed.), Analysis and Design Methods: Principles, Practice and Projects, vol. 2. Pergamon Press Ltd., Oxford, UK, pp. 245–261.
Helm, P.R., Davie, C.T., Glendinning, S., 2013. Numerical modelling of shallow abandoned mine working subsidence affecting transport infrastructure. Eng. Geol. 154, 6–19.
Ingard, U., Kraushaar, W.L., 1960. Introduction to Mechanics, Matter and Waves. Addison-Wesley, London, UK.
Jaeger, J.C., Cook, N.G.W., Zimmerman, R.W., 2007. Fundamentals of Rock Mechanics, fourth ed. Blackwell Publishing, London, UK.
Jiang, M., Jiang, T., Crosta, G.B., Shi, Z., Chen, H., Zhang, N., 2015. Modeling failure of jointed rock slope with two main joint sets using a novel DEM bond contact model. Eng. Geol. 193, 79–96.
Kulatilake, P.H.S.W., Shreedharan, S., Sherizadeh, T., Shu, B., Xing, Y., He, P., 2016. Laboratory estimation of rock joint stiffness and frictional parameters. Geotech. Geol. Eng. 34 (6), 1723–1735.
Li, J.C., 2013. Wave propagation across non-linear rock joints based on time-domain recursive method. Geophys. J. Int. 193, 970–985.
Li, J.C., Li, H.B., Jiao, Y.Y., Liu, Y.Q., Xia, X., Yu, C., 2014. Analysis for oblique wave propagation across filled joints based on thin-layer interface model. J. Appl. Geophys. 102, 39–46.
Li, J.C., Li, H.B., Zhao, J., 2015. An improved equivalent viscoelastic medium method for wave propagation across layered rock masses. Int. J. Rock Mech. Min. Sci. 73 (1), 62–69.
Li, J.C., Li, N.N., Li, H.B., Zhao, J., 2017. An SHPB test study on wave propagation across rock masses with different contact area ratios of joint. Int. J. Impact Eng. 105, 109–116.
Malama, B., Kulatilake, P.H.S.W., 2003. Models for normal fracture deformation under compressive loading. Int. J. Rock Mech. Min. Sci. 40 (6), 893–901.
Nassir, M., Settari, A., Wan, R., 2010. Joint stiffness and deformation behaviour of discontinuous rock. J. Can. Petrol. Technol. 49 (9), 78–86.
Pyrak-Nolte, L.J., 1988. Seismic Visibility of Fractures. PhD Thesis. University of California, Berkeley, USA.
Pyrak-Nolte, L.J., Myer, L.R., Cook, N.G.W., 1990. Transmission of seismic waves across single natural fractures. J. Geophys. Res. Solid Earth 95 (B6), 8617–8638.
Raven, K.G., Gale, J.E., 1985. Water flow in a natural rock fracture as a function of stress and sample size. Int. J. Rock Mech. Min. Sci. Geomech. Abstr. 22 (4), 251–261.
Schoenberg, M., 1980. Elastic wave behavior across linear slip interfaces. J. Acoust. Soc. Am. 68 (5), 1516–1521.
Scholz, C.H., Hickman, S.H., 1983. Hysteresis in the closure of a nominally flat crack. J. Geophys. Res. Solid Earth 88 (B8), 6501–6504.
Zhang, Z.H., Deng, J.H., Zhu, J.B., 2018. A rapid and nondestructive method to determine normal and shear stiffness of a single rock joint based on 1D wave-propagation theory. Geophysics 83 (1), WA89–WA100.
Zhao, J., Cai, J.G., Zhao, X.B., Li, H.B., 2006. Experimental study of ultrasonic wave attenuation across parallel fractures. Geomechanics Geoengin. 1 (2), 87–103.
Zhao, X.B., Zhu, J.B., Zhao, J., Cai, J.G., 2012. Study of wave attenuation across parallel fractures using propagator matrix method. Int. J. Numer. Anal. Methods Geo-Mech. 36, 1264–1279.
Zhu, J.B., Perino, A., Zhao, G.F., Barla, G., Li, J.C., Ma, G.W., Zhao, J., 2011. Seismic response of a single and a set of filled joints of viscoelastic deformational behaviour. Geophys. J. Int. 186, 1315–1330.
Zhu, J.B., Zhao, J., 2013. Obliquely incident wave propagation across rock joints with virtual wave source method. J. Appl. Geophys. 88, 23–30.
Zhu, J.B., Zhou, T., Liao, Z.Y., Sun, L., Li, X.B., Chen, R., 2018. Replication of internal defects and investigation of mechanical and fracture behaviours of rocks using 3D printing and 3D numerical methods with combination of X-ray computerized tomography. Int. J. Rock Mech. Min. Sci. 106, 198–212.

Dr. Zhenghu Zhang is currently an associate professor at the School of Civil Engineering, Dalian University of Technology, China. He obtained his BSc and PhD degrees from Sichuan University, China. He was a joint doctoral student at the Hong Kong Polytechnic University and is a postdoctoral fellow of Kyoto University, Japan. Dr. Zhang has hosted or participated in a number of key projects from Chinese government, such as the National Key Research and Development Program of China, the National Key Basic Research and Development Program of China (973 Program), and the National Natural Science Foundation of China. He has authored or co-authored more than 30 academic papers in international and domestic authoritative journals. His current research focuses on rock mechanics, nondestructive testing technique, stability analysis, and monitoring and early warning of rock engineering. He is a member of Chinese Society for Rock Mechanics and Engineering (CSRME) and International Society for Rock Mechanics and Rock Engineering (ISRM).